ACS APPLIED MATERIALS & INTERFACES

Research Article

www.acsami.org

Electroless Patterned Assembly of Metal Nanoparticles on Hydrogen-Terminated Silicon Surfaces for Applications in Photoelectrocatalysis

Bruno Fabre,*[,†] Leila Hennous,[†] Soraya Ababou-Girard,[‡] and Cristelle Meriadec[‡]

[†]Institut des Sciences Chimiques de Rennes, UMR 6226 CNRS/Université de Rennes 1, Matière Condensée et Systèmes Electroactifs (MaCSE), Campus de Beaulieu, 35042 Rennes Cedex, France

[‡]Institut de Physique de Rennes, UMR 6251 CNRS/Université de Rennes 1, Campus de Beaulieu, 35042 Rennes Cedex, France

ABSTRACT: The deposition of gold and platinum nanoparticles (NPs) on hydrogen-terminated Si(100) (Si(100)-H) surfaces has been performed by galvanic displacement using fluoride-free sub-millimolar metallic salt solutions. The scanning electron microscopy (SEM) images showed the formation of oblate hemispherical NPs, with an average diameter of ca. 40 nm and an average height of 20 ± 10 and 10 ± 5 nm for Au and Pt, respectively. Furthermore, the calculated number density was (6.0 ± 0.8) × 10^9 Au NPs cm^{-2} and (6.6 ± 1.3) × 10^9 Pt NPs cm^{-2} with a larger size distribution measured for Au NPs. The Au 4f and Pt 4f X-ray photoelectron spectra of the metallized surfaces were characterized by a principal component corresponding to either the metallic gold or platinum. However, two other components located at higher binding energies were also visible and ascribed to gold or platinum silicides. Using this fluoride-free deposition process and a "reagentless" UV photolithography technique, we have also demonstrated that it was possible to prepare metallic NP micropatterns. Following this approach, single metal (Au) and two metals (Au and Pt) patterns have been produced and characterized by energy-dispersive X-ray spectroscopy (EDS) which revealed the presence of the expected metal(s). Such metallic NP micropatterned surfaces were used as photocathodes for H_2 evolution from water as a proof-of-concept experiment. These electrodes exhibited much higher electrocatalytic performance than that of nonmetallized Si(100)-H, both in the absence of light and under illumination. The overpotential for hydrogen evolution was significantly decreased by ca. 450 mV with respect to Si(100)-H (measured for a current density of 0.1 mA cm^{-2}) under identical illumination conditions.

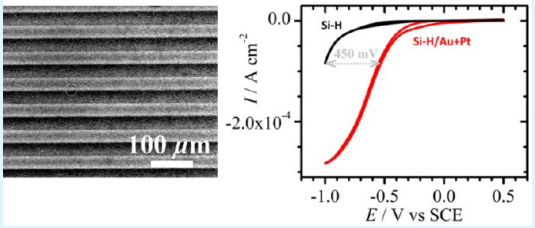

KEYWORDS: *gold nanoparticles, platinum nanoparticles, galvanic displacement, silicon surfaces, electrocatalysis, electron microscopy (SEM), electron spectroscopy (XPS)*

1. INTRODUCTION

The electroless deposition of metallic nanoparticles (NPs) onto semiconducting surfaces by galvanic displacement has been demonstrated to be a powerful, simple, and fast method to produce metallized surfaces with a high density of NPs.[1−10] Such surfaces could find applications in electronic circuit devices,[11−13] photoelectrocatalysis,[14] optoelectronics,[15,16] and others.[17] The deposition by galvanic displacement occurs spontaneously if the redox potential of the tested metallic couple is higher than those of both the semiconducting surface and the hydrogen evolution. For instance, the spontaneous deposition of noble metals, such as gold, platinum, or palladium, onto oxide-free silicon is expected in the presence of the corresponding gold(III), platinum(II), or palladium(II) salt if we refer to the redox potentials of the Au^{3+}/Au, Pt^{2+}/Pt, Pd^{2+}/Pd, and SiF_6^{2-}/Si redox couples, namely, 1.42, 1.20, 0.83, and −1.20 V vs NHE, respectively.[18] Usually, hydrogen fluoride is added in the metallic salt solution to ensure continuous metallic growth. Under these conditions, the semiconductor acts as a source of electrons that reduce the metallic salt to metal on the surface, and silicon is oxidized spontaneously into soluble hexafluoride silicon salt (Scheme 1). Although this method has been largely developed, the principal drawback of this approach is related to some difficulties of controlling both the density and the morphology of deposited particles. On the opposite, only few studies have been concerned with the electroless deposition of metal nanostructures by galvanic displacement using solutions of metallic salts without fluorinated species.[2,6,19−22] This approach was demonstrated to be efficient for producing various metallic (Au, Ag, and Ni) NPs on silicon as well as ultrathin and ultrasmooth metallic films. Furthermore, the investigation of the physical and

Scheme 1. Principle of the Spontaneous Electroless Deposition of Metallic Nanoparticles onto Oxide-Free Hydrogen-Terminated Silicon (Si−H) by Galvanic Displacement (Left) in the Presence and (Right) in the Absence of Hydrogen Fluoride

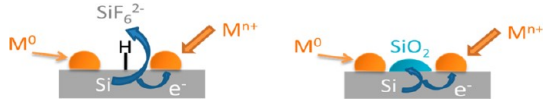

Received: October 5, 2012
Accepted: December 30, 2012
Published: December 31, 2012

chemical properties of the metal NP−silicon interface revealed that the fluoride-free deposition resulted in the formation of silicides,[19] although this statement is still controversial. The advantage of the fluoride-free method is that the deposition process is inherently self-limiting. Under these conditions, the growth of metal nanoparticles is stopped when the electron transfer between the silicon and the metallic cation is blocked by the insulating SiO_x layer which cannot be dissolved. In the present work, we demonstrate for the first time that the fluoride-free deposition method is perfectly suitable for fabricating single Au and bimetallic Au and Pt NP micropatterns on silicon when combined with an UV photolithography technique. Such metallized interfaces can be of high interest in the large area of electrochemistry (e.g., for electrocatalysis and electroanalysis) and for electrochemically switchable surface-enhanced Raman scattering (SERS).

2. EXPERIMENTAL SECTION

2.1. Reagents. Acetone (MOS electronic grade, Erbatron from Carlo Erba) and anhydrous ethanol (RSE electronic grade, Erbatron from Carlo Erba) were used without further purification. The chemicals used for cleaning and etching of silicon wafer pieces (30% H_2O_2, 96−97% H_2SO_4, and 50% HF solutions) were of VLSI semiconductor grade (Riedel-de-Haën).

2.2. Preparation of the Metallic NPs-Covered Si(100) Surfaces by Fluoride-Free Galvanic Displacement. All Teflon vials used for cleaning of silicon were previously decontaminated in 3:1 v/v concentrated H_2SO_4/30% H_2O_2 at 100 °C for 30 min, followed by copious rinsing with ultrapure water.

Caution: The concentrated H_2SO_4:H_2O_2(aq) piranha solution is very dangerous, particularly in contact with organic materials, and should be handled extremely carefully.

Double side polished silicon(100) samples (*p*-type, boron doped, 5−10 Ω cm, thickness = 250 ± 25 μm, from Siltronix) were cut into 1.5 × 1.5 cm^2 pieces from the same silicon wafer to ensure the maximum reproducibility of hydrogen-terminated surfaces. The sample was sonicated for 10 min successively in acetone, ethanol, and ultrapure 18.2 MΩ cm water (Elga Purelab Classic UV, Veolia Water STI). It was then cleaned in 3:1 v/v concentrated H_2SO_4/30% H_2O_2 at 100 °C for 30 min, followed by copious rinsing with ultrapure water. The surface was etched in aqueous HF ca. 10% for 2 min to convert the oxide to hydrogenated areas and then immersed for 5 min in an aqueous metallic salt solution containing hydrogen tetrachloroaurate(III) hydrate $HAuCl_4$ (Strem Chemicals) or sodium tetrachloroplatinate(II) hydrate Na_2PtCl_4 (Strem Chemicals) at 0.3 mM. The surface was thoroughly rinsed with ultrapure water and dried under an argon stream.

2.3. Micropatterning of Metallic NPs Deposited on Si(100) Surfaces. The surface Si(100)-H was irradiated through a photomask (20 μm wide dark lines separated by 40 μm or 10 μm diameter dark disks separated by 30 μm; the mask from DelfMEMS S.A.S, France, is chromium on quartz with an antiscratch coating) with UV light (Hg(Ar) pen lamp, UVP, model 11SC-1, ca. 4.5 mW cm^{-2}) for 30 min under ambient conditions. It was then immersed immediately into the aqueous $HAuCl_4$ solution at 0.3 mM for 5 min. The surface was thoroughly rinsed with ultrapure water and dried under an argon stream. For the deposition of the second metal, the Au NP-micropatterned surface was dipped in aqueous HF ca. 10% for 2 min and then immersed for 5 min in the aqueous Na_2PtCl_4 solution at 0.3 mM. The surface was thoroughly rinsed with ultrapure water and dried under an argon stream.

2.4. Surface Characterizations. *X-ray Photoelectron Spectroscopy (XPS) Analysis.* After a few minutes exposure to ambient atmosphere, the modified surfaces were introduced in the UHV chamber and kept at 1 × 10^{-9} mbar for several hours before XPS analysis. XPS measurements were performed with a Mg Kα ($h\nu$ = 1254 eV) X-ray source, using a VSW HA100 photoelectron spectrometer with a hemispherical photoelectron analyzer, working at an energy pass of 22 eV. The experimental resolution was then 1.0 eV. Spectral analysis included a Shirley background subtraction and peak separation using mixed Gaussian−Lorentzian functions. Note that the Si 2p signal measured before and after deposition was averaged over several emission angles around normal emission to eliminate photoelectron diffraction effects.

Scanning Electron Microscopy (SEM) and Energy-Dispersive X-ray Spectroscopy (EDS) Measurements. The SEM images were taken with a JSM-6400 JEOL scanning electron microscope, and the EDS analysis was performed with a similar setup equipped with the WDS/EDS system.

Electrochemical Characterizations. Cyclic voltammetry measurements were performed with an Autolab electrochemical analyzer (PGSTAT 30 potentiostat/galvanostat from Eco Chemie B.V.) equipped with the GPES software in a homemade three-electrode Teflon cell. The working electrode, bare or metallic NP-covered Si(100), was pressed against an opening in the cell bottom using an FETFE (Aldrich) O-ring seal. An ohmic contact was made on the previously polished rear side of the sample by applying a drop of an In−Ga eutectic (Alfa-Aesar, 99.99%). The electrochemically active area of the Si(100) surface was 0.3 cm^2. The counter electrode was a platinum grid, and aqueous SCE was used as the reference electrode. All electrochemical measurements were carried out inside a homemade Faraday cage, at room temperature (20 ± 2 °C) and under constant argon flow, either in the dark or under illumination using an optical fiber (Olympus, Highlight 2100, maximum power). The resistance of the electrolytic cell was compensated by positive feedback.

3. RESULTS AND DISCUSSION

Figure 1 shows the SEM images of Au and Pt NPs deposited on Si(100)-H by electroless galvanic displacement from an aqueous metallic solution at 0.3 mM. The resulting NPs are of oblate hemispherical shape, with an average diameter of 42 and 41 nm and an average height (as determined by atomic force microscopy, data not shown) of 20 ± 10 and 10 ± 5 nm for Au and Pt, respectively. Furthermore, the number density calculated from SEM was (6.0 ± 0.8) × 10^9 Au NPs cm^{-2} and (6.6 ± 1.3) × 10^9 Pt NPs cm^{-2} with a larger size distribution measured for Au NPs (the width at half-maximum is found to be 35 and 16 nm for Au and Pt NPs, respectively). Under fluoride-free deposition conditions, it can be thus concluded that the total number of moles of deposited Au NPs is higher than that of Pt NPs in spite of rather similar morphological characteristics.

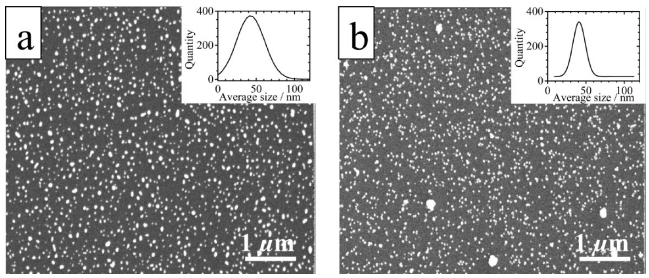

Figure 1. SEM images of (a) Au and (b) Pt NPs on Si(100)-H prepared by fluoride-free electroless deposition. The surface was immersed in an aqueous 0.3 mM $HAuCl_4$ or Na_2PtCl_4 solution for 5 min. The insets correspond to the particle size distributions.

Further information on both the composition and the oxidation states of the deposited NPs and the underlying silicon surface can be provided by the X-ray photoelectron spectroscopy (XPS) analysis of the metallized surfaces. For the Au NP-covered surface, the Au 4f core level spectrum shows one principal component characterized by its respective $4f_{5/2}$ and

dx.doi.org/10.1021/am302226q | ACS Appl. Mater. Interfaces 2013, 5, 338−343

$4f_{7/2}$ levels at 87.8 and 84.2 eV, which can be assigned to the metallic gold by comparison with a Au foil as reference (Figure 2). However, two other components located at higher binding

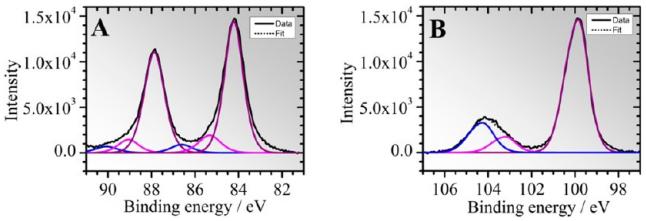

Figure 2. XPS Au 4f (A) and Si 2p (B) resolved spectra of Au NP-covered Si(100)-H surfaces. The experimental data are the solid black lines. Dotted black lines are the fitted curves using three Gaussian–Lorentzian mixed components corresponding to different gold (A) and silicon (B) states.

energies (namely, 89.1 and 85.3 eV for the first component and 90.1 and 86.6 eV for the less intense second one) were required to fit correctly the experimental spectrum. These new features can be ascribed to gold silicides (Au_xSi) in good agreement with literature data.[19,23−27] The experimental ratio between the peak areas of the metallic Au and Au_xSi components is estimated at 5. Moreover, the Si 2p signal shows as expected the presence of a principal component at 99.8 eV attributed to Si–Si bonds and an intense peak due to silicon oxides at a binding energy of about 104 eV.

For the Pt NP-covered surface, the Pt 4f spectrum shows the presence of metallic Pt characterized by its two 5/2 and 7/2 levels at 74.5 and 71.2 eV (Figure 3). Two other components at

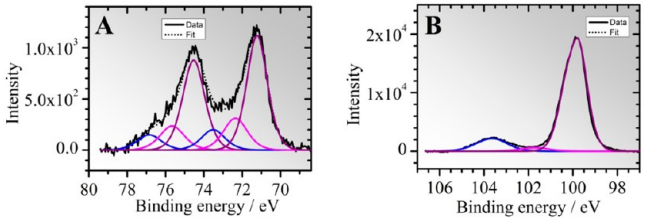

Figure 3. XPS Pt 4f (A) and Si 2p (B) resolved spectra of Pt NP-covered Si(100)-H surfaces. The experimental data are the solid black lines. Dotted black lines are the fitted curves using three Gaussian–Lorentzian mixed components corresponding to different platinum (A) and silicon (B) states.

76.8 (73.5) and 75.7 eV (72.3) for the $4f_{5/2}$ ($4f_{7/2}$) levels are also involved in the fitting of the experimental spectrum. The positions of these two additional features are indicative of the presence of PtSi[28,29] and Pt_2Si[30] forms, respectively, coexisting with Pt. The experimental ratio between the areas under the metallic Pt and Pt_xSi peaks is ca. 2. Compared with Au NPs, the larger spectral proportion of silicides found for the Pt NPs as well as the smaller proportion of silicon oxides relative to that of the Si–Si feature in the Si 2p spectrum (Figure 3b) suggest that the total number of moles of Pt NPs deposited on Si(100) is smaller than that of Au NPs, in perfect line with SEM data. This is also corroborated by the atomic ratios between the sensitivity factor-normalized peak areas of total metal (Au or Pt) and total Si signals, namely, 0.06 and 7.5×10^{-3} for Au and Pt NPs, respectively.

Having demonstrated that the fluoride-free deposition process was convenient to metallize uniformly hydrogenated Si(100) surfaces, this approach has been further exploited for locally depositing metallic NPs on silicon. The strategy used is depicted in Scheme 2 and is based on the photochemical

Scheme 2. Micropatterning of Si–H Surfaces by Single Metal (Au) and Two Metals (Au and Pt) NPs Using UV Photolithography Combined with Electroless Metallic Deposition by Galvanic Displacement[a]

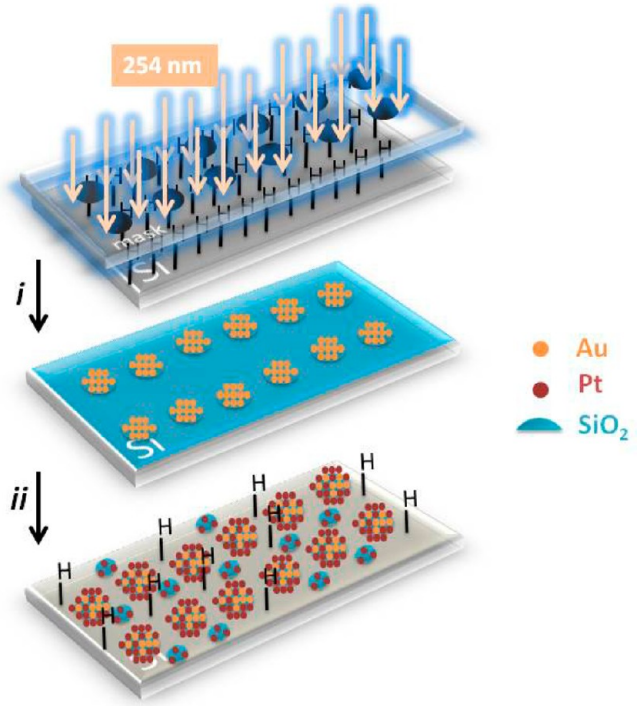

[a]Reagents and conditions: (i) irradiation at 254 nm for 30 min, then immersion in 0.3 mM $HAuCl_4$ for 5 min; (ii) immersion in HF ca. 10% for 2 min, then immersion in 0.3 mM Na_2PtCl_4 for 5 min.

oxidation of Si(100)-H through an optical mask. The Si(100)-H surface was irradiated at 254 nm through a mask in ambient air for 30 min converting the exposed area into silicon oxide. The unexposed area, which remains hydrogen terminated, is then covered selectively with metallic NPs, namely, gold, after immersion of the micropatterned surface in the metallic solution.

SEM images shown in Figure 4 clearly reveal the patterns, and the energy-dispersive X-ray spectroscopy (EDS) analysis shows the presence of the expected metal (Figure 5). The resolution in Figure 4 confirms that the pattern transfer is limited by the quality of the optical system (proximity mask in this case). Compared with uniformly modified surfaces, it can be noticed that the morphology of the metallic microstructures is somewhat different. Such a result can be essentially ascribed to differences in local redox potential between uniformly hydrogenated and SiO_2/Si–H micropatterned silicon surfaces which are thought to change the rate of the growth mechanism.

As already demonstrated for photochemically micropatterned silicon surfaces,[31−34] an interest of this lithographic method is that the silicon oxide patterns can be selectively dissolved in diluted HF solution to generate newly potentially reactive hydrogenated areas. However, it must be kept in mind that both photochemically generated silicon oxide areas and those surrounding the Au nanoparticles will be converted to

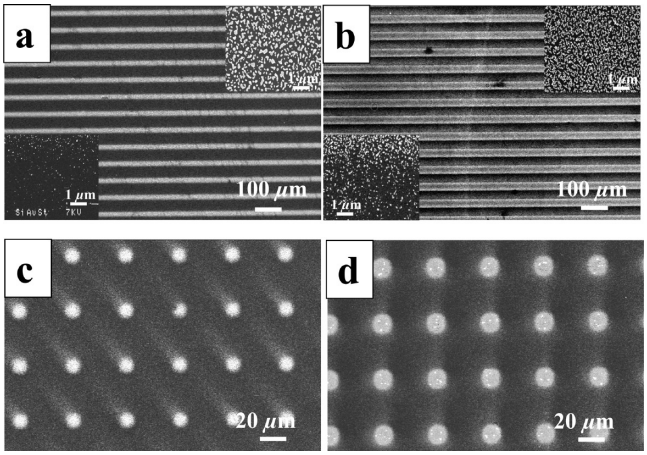

Figure 4. SEM images of (a,c) Au and (b,d) Au and Pt NP micropatterns deposited on Si(100)-H surfaces. The insets in a and b correspond to higher magnifications of nanoparticles deposited inside (top right corner) and between (bottom left corner) the lines. The photomask contains 20 μm wide lines separated by 40 μm (a,b) or 10 μm diameter disks separated by 30 μm (c,d).

hydrogenated areas. Interestingly, these hydrogenated patterns can then be used for the selective deposition of a second metal (namely, Pt) after exposure of this sample to a $PtCl_4^{2-}$ solution. As shown in Figure 4, the density of Pt particles was found to be higher inside the predeposited Au patterns than inside the hydrogenated spacings, as confirmed by the EDS analysis (Figure 5). Such a result is not unexpected and can be reasonably well explained by the electrochemical activation of the Pt deposition process by the predeposited conducting gold features. Indeed, as demonstrated by Osaka and co-workers,[35] the deposition of the second metal is expected to take place on top of the nuclei of the existing metal. Additionally, we can also notice that the quantity of predeposited Au remained approximately constant after treatment with HF and deposition of the second metal, which indicates the absence or a minority proportion of a silicon oxide interface between silicon and deposited gold.

To examine if such metal/silicon interfaces could be of interest for electrochemical catalysis, we have used the metallic NP micropatterned surfaces as photocathodes for H_2 evolution from water as a proof-of-concept experiment. As shown in Figure 6, such electrodes exhibited much higher electrocatalytic performance than that of nonmetallized Si(100)-H, both in the absence of light and under illumination. For example, the overpotential for hydrogen evolution was significantly decreased by ca. 450 mV with respect to Si(100)-H (measured for a current density of 0.1 mA cm^{-2}) under identical illumination conditions. Furthermore, the measured electrochemical current intensities were considerably increased upon illumination, as expected for a reduction process occurring at a *p*-type semiconductor. The fact that both current values in the dark were higher than those measured at a bare Si(100)-H and the current values were dramatically increased by switching from the dark to illumination indicates an efficient interfacial charge transport which is consistent with the absence or the negligible contribution of a thin oxide barrier at the metal−Si(100)

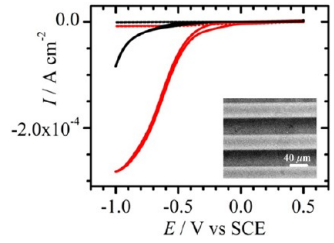

Figure 6. Cyclic voltammograms at 0.02 V s^{-1} of bare (black) and Au and Pt NP lines micropatterned (red) *p*-type Si(100)-H surfaces in 0.1 M aq H_2SO_4, in dark (dotted lines) and under illumination (solid lines).

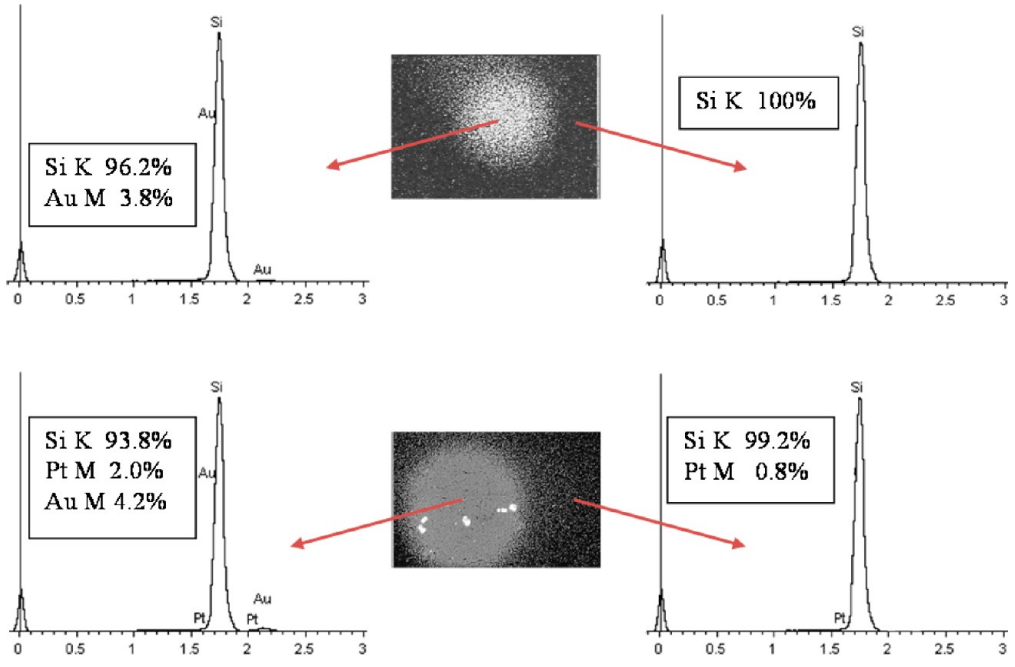

Figure 5. EDS spectra taken inside and outside the patterns of single Au (top) and Au and Pt (bottom) NP-covered 10 μm diameter disks deposited on Si(100)-H surfaces. The percentages are w/w.

dx.doi.org/10.1021/am302226q | ACS Appl. Mater. Interfaces 2013, 5, 338−343

interface. Indeed, if an insulating electrically oxide layer was present between silicon and metallic NPs, it is very likely that the interfacial charge transport would have been dramatically inhibited.

4. CONCLUSIONS

In conclusion, the fluoride-free electroless deposition by galvanic displacement combined with a UV photolithography method has been used for micrometer scale patterning of metallic NPs on Si(100)-H surfaces. Using this simple and versatile process, we have demonstrated the ability to fabricate single Au and bimetallic Au and Pt NP micropatterns. Such a micropatterning approach would not be compatible with the commonly developed metallic deposition method involving HF because the oxide patterns photochemically generated in our lithographic process would be erased after immersion of silicon in the fluoride solution. There are also other advantages to this convenient and flexible lithographic approach involving Si-H/SiO_x micropatterned silicon surfaces. In this work, silicon oxide patterns have been dissolved to deposit a second metal on the silicon surface. However, for some applications, it may be convenient to react the generated oxide patterns with some organosilane derivatives (trialkoxy- and trichlorosilanes) to introduce patterned assemblies of functional molecules to metallic NP-coated silicon. Also interestingly, the immobilized metallic NPs could be also used to introduce organic function to the semiconductor surface using surface chemistry reactions compatible with the deposited metal (for example, self-assembly with organothiolates). In this study, the metallized interfaces were found to be efficient for the photoelectrocatalytic reduction of protons to dihydrogen, as a proof-of-concept experiment. Besides applications in electrochemical catalysis, such interfaces could also be of interest for the fabrication of metallic interconnects and electrode networks for the electrochemical sensing but also for the controlled cell adhesion and growth. Moreover, because both the size and the morphology of deposited metallic NPs are ideal for efficient SERS,[36−40] the SERS activity of our metallized surfaces using different organothiolates as analytes is underway, and the results corresponding to this study will be published elsewhere.

AUTHOR INFORMATION

Corresponding Author

*E-mail: fabre@univ-rennes1.fr.

Notes

The authors declare no competing financial interest.

ACKNOWLEDGMENTS

Financial support from the CNRS and UMR 6226 is gratefully acknowledged. Dr. J. Le Lannic and I. Peron from "Centre de Microscopie Electronique à Balayage et microAnalyse" (CMEBA) are fully thanked for the SEM and EDS measurements.

REFERENCES

(1) Sayed, S. Y.; Wang, F.; Malac, M.; Meldrum, A.; Egerton, R. F.; Buriak, J. M. *ACS Nano* **2009**, *3*, 2809−2817.
(2) Zhang, X.; Qiao, Y.; Xu, L.; Buriak, J. M. *ACS Nano* **2011**, *5*, 5015−5024.
(3) Porter, L. A.; Choi, H. C.; Schmeltzer, J. M.; Ribbe, A. E.; Elliott, L. C. C.; Buriak, J. M. *Nano Lett.* **2002**, *2*, 1369−1372.
(4) Hormozi Nezhad, M. R.; Aizawa, M.; Porter, L. A., Jr.; Ribbe, A. E.; Buriak, J. M. *Small* **2005**, *1*, 1076−1081.
(5) Ferralis, N.; Maboudian, R.; Carraro, C. *J. Phys. Chem. C* **2007**, *111*, 7508−7513.
(6) Magagnin, L.; Maboudian, R.; Carraro, C. *J. Phys. Chem. B* **2002**, *106*, 401−407.
(7) Carraro, C.; Maboudian, R.; Magagnin, L. *Surf. Sci. Rep* **2007**, *62*, 499−525 and references therein.
(8) Sun, Y. *Adv. Funct. Mater.* **2010**, *20*, 3646−3657.
(9) Warren, S.; Reitzle, A.; Kazimirov, A.; Ziegler, J. C.; Bunk, O.; Cao, L. X.; Renner, F. U.; Kolb, D. M.; Bedzyk, M. J.; Zegenhagen, J. *Surf. Sci.* **2002**, *496*, 287−298.
(10) Nagahara, L. A.; Ohmori, T.; Hashimoto, K.; Fujishima, A. *J. Vac. Sci. Technol. A* **1993**, *11*, 763−767.
(11) Ieong, M.; Doris, B.; Kedzierski, J.; Rim, K.; Yang, M. *Science* **2004**, *306*, 2057−2060.
(12) Wu, Y.; Xiang, J.; Yang, C.; Lu, W.; Lieber, C. M. *Nature* **2004**, *430*, 61−65.
(13) Li, B.; Luo, Z. Q.; Shi, L.; Zhou, J. P.; Rabenberg, L.; Ho, P. S.; Allen, R. A.; Cresswell, M. W. *Nanotechnology* **2009**, *20*, 1−7.
(14) Boettcher, S. W.; Warren, E. L.; Putnam, M. C.; Santori, E. A.; Turner-Evans, D.; Kelzenberg, M. D.; Walter, M. G.; McKone, J. R.; Brunschwig, B. S.; Atwater, H. A.; Lewis, N. S. *J. Am. Chem. Soc.* **2011**, *133*, 1216−1219.
(15) Ootsuka, T.; Liu, Z. X.; Osamura, M.; Fukuzawa, Y.; Otogawa, N.; Nakayama, Y.; Tanoue, H.; Makita, Y. *Mater. Sci. Eng., B* **2005**, *124*, 449−452.
(16) Giziewicz, W. P.; Fonstad, C. G. *Vac. Sci. Technol. A* **2002**, *20*, 1052−1056.
(17) Lin, K. W.; Chen, H. I.; Lu, C. T.; Tsai, Y. Y.; Chuang, H. M.; Chen, C. Y.; Liu, W. C. *Semicond. Sci. Technol.* **2003**, *18*, 615−619.
(18) Lide, D. R. *CRC Handbook of Chemistry and Physics*, 87th ed.; Taylor and Francis: Boca Raton, 2007.
(19) Zhao, L.; Chung-Lung Siu, A.; Petrus, J. A.; He, Z.; Leung, K. T. *J. Am. Chem. Soc.* **2007**, *129*, 5730−5734.
(20) Gutés, A.; Carraro, C.; Maboudian, R. *ACS Appl. Mater. Interfaces* **2011**, *3*, 1581−1584.
(21) Ye, W. C.; Tong, H.; Wang, C. M. *Microchim. Acta* **2005**, *152*, 85−88.
(22) Osaka, T.; Takano, N.; Komaba, S. *Chem. Lett.* **1998**, *27*, 657−658.
(23) Sundaravel, B.; Sekar, K.; Kuri, G.; Satyam, P. V.; Dev, B. N.; Bera, S.; Narasimhan, S. V.; Chakraborty, P.; Caccavale, F. *Appl. Surf. Sci.* **1999**, *137*, 103−112.
(24) Khalfaoui, R.; Benazzouz, C.; Guittoum, A.; Tabet, N.; Tobbeche, S. *Vacuum* **2006**, *81*, 45−48.
(25) Sarkar, D. K.; Bera, S.; Dhara, S.; Narasimhan, S. V.; Chaudhury, S.; Nair, K. G. M. *Solid State Commun.* **1998**, *105*, 351−356.
(26) Dahal, N.; Wright, J. T.; Willey, T. M.; Meulenberg, R. W.; Chikan, V. *ACS Appl. Mater. Interfaces* **2010**, *2*, 2238−2247.
(27) It has been demonstrated from high-resolution transmission electron microscopy combined with nanobeam diffraction measurements that the deposition of Au NPs on Si(100) by galvanic displacement in the presence of fluoride resulted in the formation of numerous gold silicides Au_x Si with x going from 2 to 7 (ref 1). Such intermetallics which are composed of Au at different oxidation states should give rise to several components in the Au 4f spectrum at higher binding energies than that for metallic Au.
(28) Gorostiza, P.; Servat, J.; Morante, J. R.; Sanz, F. *Thin Solid Films* **1996**, *275*, 12−17.
(29) Cerruti, M.; Doerk, G.; Hernandez, G.; Carraro, C.; Maboudian, R. *Langmuir* **2010**, *26*, 432−437.
(30) Briggs, D.; Seah, M. P. *Practical Surface Analysis: Auger and X-Ray Photoelectron Spectroscopy*, 2nd ed.; Wiley & Sons: Chichester, 1993; Vol. *1*.
(31) Wojtyk, J. T. C.; Tomietto, M.; Boukherroub, R.; Wayner, D. D. M. *J. Am. Chem. Soc.* **2001**, *123*, 1535−1536.
(32) Mischki, T. K.; Donkers, R. L.; Eves, B. J.; Lopinski, G. P.; Wayner, D. D. M. *Langmuir* **2006**, *22*, 8359−8365.
(33) Fabre, B.; Wayner, D. D. M. *Langmuir* **2003**, *19*, 7145−7146.
(34) Fabre, B.; Herrier, C. *RSC Adv.* **2012**, *2*, 168−175.

(35) Niwa, D.; Homma, T.; Osaka, T. *J. Phys. Chem. B* **2004**, *108*, 9900−9904.
(36) Bechelany, M.; Brodard, P.; Elias, J.; Brioude, A.; Michler, J.; Philippe, L. *Langmuir* **2010**, *26*, 14364−14371.
(37) Wang, Y.; Becker, M.; Wang, L.; Scholz, R.; Peng, J.; Gösele, U.; Christiansen, S.; Kim, D. H.; Steinhart, M. *Nano Lett.* **2009**, *9*, 2384−2389.
(38) Gutés, A.; Carraro, C.; Maboudian, R. *ACS Appl. Mater. Interfaces* **2009**, *1*, 2551−2555.
(39) Gutés, A.; Carraro, C.; Maboudian, R. *J. Am. Chem. Soc.* **2010**, *132*, 1476−1477.
(40) Sun, Y.; Wiederrecht, G. P. *Small* **2007**, *3*, 1964−1975.